Electronic structure and vibrational properties of Ba_8Si_{46}, $Ba_8Ag_nSi_{46-n}$, and $Ba_8Au_nSi_{46-n}$

J. S. Tse
Department of Physics and Engineering Physics, University of Saskatchewan, Saskatoon, Canada S7N 5E2

T. Iitaka
Computational Astrophysics Lab, RIKEN, 2-1 Hirosawa, Wako, Saitama, 351-0198, Japan

T. Kume and H. Shimizu
Department of Materials Science, Gifu University, 1-1 Yanagido, Gifu 501-1193, Japan

K. Parlinski
Institute of Nuclear Physics, Polish Academy of Sciences, ul.Radzikowskiego 152, 31-342 Cracow, Poland

H. Fukuoka and S. Yamanaka
Department of Applied Chemistry, Graduate School of Engineering, Hiroshima University, Higashi-Hiroshima, 739-8527, Japan
(Received 13 June 2005; revised manuscript received 10 August 2005; published 28 October 2005)

The electronic and vibrational structures of Ba_8Si_{46} and $Ba_8M_nSi_{46-n}$, where some of the framework Si were replaced by metal (M=Ag or Au) have been studied. Theoretical calculations show that the nature of chemical bonding of the substituted clathrates and their vibrational properties are fundamentally different from Ba_8Si_{46}. Low-frequency vibrations associated with the motions of Ba in the large cages and the framework metals have been identified from their Raman spectra. A surprisingly large contribution of the low-frequency modes, particularly those which arise from the Ba vibrations in the large cages, to the electron-phonon coupling parameter in Ba_8Si_{46} was found.

DOI: 10.1103/PhysRevB.72.155441 PACS number(s): 78.30.−j, 63.20.Dj, 63.20.Pw, 71.20.−b

I. INTRODUCTION

Since the discovery of superconducting behavior in Na and Ba doped silicon clathrates,[1,2] the electronic structure and properties of this novel polyhedral network compounds have been a subject of intense study by both theory and experiment. It is found that the superconductivity is sensitive to the encapsulated metal and also on the atoms forming the framework. The superconducting critical temperature was found to decrease if the Ba is replaced by a Na atom[1,2] or Sr atom.[3] Furthermore, the substitution of noble metals, such as Ag and Au, also decrease the critical temperature.[4,5] Several recent investigations have shed light on the mechanism for the superconductivity. Through the comparison of the Raman spectra of Ba_8Si_{46} and $Ba_8Au_6Si_{40}$, it was suggested[6] that the dominant vibrational mode responsible for strong electron-phonon coupling in Ba_8Si_{46} (Cooper pairing) is the highest energy Si stretching vibration at 437 cm^{-1}. This assertion, however, contradicts with the rather small calculated electron-phonon coupling (or mass enhancement) parameter (λ) for this mode.[7] However, theoretical calculations, performed only for the zone center phonon modes, show that almost all phonon modes contribute to the electron coupling process and there are significant contributions coincidences with the encapsulated metal "localized" modes at low frequencies.[7] For this reason, the calculated $\langle\omega_{\log}\rangle$ prefactor of 450 K is in agreement with the use of the experimental mean frequency in the range 191–437 cm^{-1}. It is remarkable that a very similar λ of 0.79–1.2 was obtained from Raman analysis of the isotope shifts.[6,7] Using the McMillan equation,[8]

$$T_c = \frac{\langle\omega_{\log}\rangle}{1.20}\exp\left[\frac{-1.04(1+\lambda)}{\lambda-\mu^*(1+0.62\lambda)}\right]$$

and equating the experimental critical temperature (T_c) with λ, a Coulomb potential parameter μ^* of ~0.23–0.31 was obtained. This value agrees well with the theoretical predicted value of 0.24. Other studies also show that the change in superconducting temperature also correlates very well with the electron density of states near the Fermi level. Despite the apparent good agreement between theory and results obtained from the analysis of the Raman spectra, the role of the encapsulated metal atoms and the effects of substituting the framework Si with noble metals is still not entirely clear.[9] To further the understanding of the interactions between the encapsulated metal with the framework with and without substitution, we performed a complementary experimental and theoretical investigation. First-principles calculations were used to obtain the electronic and phonon band structures for selected Si clathrates. The calculated vibrational densities are then compared with experimental Raman spectra.

II. EXPERIMENTAL AND THEORETICAL DETAILS

A. Sample preparation and Raman spectroscopy[10]

Ternary Si clathrates of $Ba_8Ag_6Si_{40}$ and $Ba_8Au_nSi_{46-n}$ (n=1,3–6) were synthesized with a high pressure technique similar to that established for Ba_8Si_{46}.[2,11] Barium (Ba), silver (Ag) [or gold (Au)], and silicon (Si) were mixed in the given atomic stoichiometry (for example, in the mole ratio 8:6:40

for $Ba_8Ag_6Si_{40}$) and are melted in an arc furnace under Ar atmosphere. The melted mixtures were ground and packed into a hexagonal Boron Nitride (*h*-BN) cell. The BN cell was compressed under a pressure of 3 GPa and heated to 800°C for 30 min followed by rapid quenching to room temperature. The integrity of the samples was characterized with powder x-ray diffraction (XRD) measurements. The obtained XRD spectra were consistent with previous data for Ba-Ag-Si and Ba-Au-Si ternary clathrates.[12,13] Raman spectra of the samples were measured at atmospheric temperature and pressure in a backscattering geometry with a micro-Raman spectrometer (JASCO NR 1800) equipped with a triple polychromator and a charge coupled device detector. Radiation of 532 nm from a solid state laser (Coherent Verdi) was used for the excitation of the Raman spectra. The spectral resolution was about 1 cm^{-1}. In order to remove undesirable Raman lines of gaseous N_2 and O_2 rotation below 200 cm^{-1}, the sample was placed in a cell filled with helium gas.

B. First-principles calculations

First-principles density function calculations were performed using the Vienna *ab initio* simulation package (VASP).[14] The atom projector augmented wave (PAW) pseudopotentials[15] were taken from the pseudopotential library provided with the software package.[14] Phonon band structures were computed with the supercell method on fully optimized geometries. The supercell method[16–18] has been applied with success in the study of the vibrational properties of Si and related clathrates.[19,20] A Monkhorst-Pack $4\times4\times4$ *k*-point set was used in all the calculations. To minimize errors in the calculation of the Hellmann-Feynman forces, the total energy was converged to better than 10^{-7} eV. In view of the large unit cell size ($\sim$10 Å) of the Si clathrates, only a single crystallographic cell was employed. This seems to be a good approximation as the analysis of the force constants show that the interplanar force constants decrease rapidly with the distance. The phonon band structures for the high symmetry ($Pm3n$) Ba_8Si_{46}, $Ba_8Au_6Si_{40}$, and $Ba_8Ag_6Si_{40}$ were studied. In the latter two compounds, the Au and Ag atoms replace the Si in the 6*c* sites.[12,13] For Ba_8Si_{46}, the calculated vibrational frequencies at the Brillouin zone center were checked against a linear response calculation and good agreement was found. The phonon dispersion curves along symmetry directions in the first Brillouin zone were generated from the calculated force constants. From previous experience on similar clathrate systems,[20,21] particularly, from the excellent comparison of calculated and experimental heat capacity on Na_8Si_{46},[21] we expected the theoretical phonon spectra presented here should be of comparable accuracy. To further investigate the electron phonon coupling mechanism in Ba_8Si_{46}, the contribution of both Ba and Si atoms to the electron phonon coupling parameter (λ) were calculated from the zone-center phonons using the program[22] PWSCF following the procedure described in Ref. 7.

The effects of substituting the framework Si with one, three, and six Ag in the 6*c* sites on the electronic band structure were studied in detail. Calculations were made on the optimized structure of $Ba_8Ag_6Si_{40}$. The lowering of the crystal symmetry demanded much larger computing resources and these calculations were performed with the pseudopotential program SIESTA employing localized basis sets.[23] It is noteworthy that both VASP and SIESTA produce almost identical crystal and electron band structures for the Si clathrates. The optimized unit cell size for Ba_8Si_{46}, $Ba_8Ag_6Si_{40}$, and $Ba_8Au_6Si_{40}$ with VASP were 10.402 Å, 10.560 Å, and 10.513 Å, respectively. These values compare well with those obtained from SIESTA of 10.421 Å, 10.557 Å, and 10.532 Å. The experimental unit cell constant for Ba_8Si_{46} is 10.328 Å.[2]

III. RESULTS AND DISCUSSIONS

A. Electronic structure

Results of the present electronic structure calculations for Ba_8Si_{46} are in good agreement with those reported in the literature.[17,24] Strong hybridization of the valence states of Ba with the conduction band of the Si_{46} framework led to a maximum in the electron density of states (DOS) near the Fermi level. Instead of repeating the analysis which has already been reported,[17] we focus on the subtle changes in the electronic DOS in the series $Ba_8Ag_nSi_{46-n}$ ($n=0$, 1, 3, and 6). The results are compared with recent photoelectron (PE) spectra obtained with synchrotron radiation with photon energy $\sim$800 eV at 20 K.[5] Soft x-ray photoelectron spectroscopy is a powerful tool for the investigation of the valence bulk states of solids where the contribution from surface states can be eliminated. Figure 1(a) shows the calculated DOS of Ba_8Si_{46} from 0 to 10 eV. The theoretical valence level DOS can be divided into four bands. The DOS shows a sharp peak with a distinct shoulder near the Fermi level. This is followed by a band centered at $\sim$3.5 eV with a full width at half maximum (FWHM) of 2.7 eV. Another band with a narrower width of 1.2 eV is located at 6.5 eV. Finally, a broad band centered around 9.5 eV with half-width range from 8 to 11 eV. The agreement between the calculated DOS of Ba_8Si_{46} with the experimental PE spectrum[5] is exceedingly good. Both the position and the width of the PE bands are well reproduced. It is reassuring that even the weak shoulder of the first band observed in the PE spectrum is reproduced correctly.

The calculated DOS convoluted with the instrumental resolution of 175 meV (Ref. 5) for $Ba_8Ag_nSi_{46-n}$ ($n=0$, 1, 3, and 6) near the Fermi level (0–3 eV) are compared in Fig. 1(b). The most distinctive feature of this DOS is the gradual decrease of the density of states with increasing Ag content in the framework. The very sharp peak near the Fermi level in Ba_8Si_{46} has reduced to a weak shoulder in $Ba_8Ag_6Si_{46}$. Furthermore, significant changes in the DOS around 2–3 eV are observed. Once again the band located at $\sim$2.4 eV broadens significantly with increasing Ag content. The calculated changes in the density of states features in the series $Ba_8Ag_nSi_{46-n}$ ($n=0$, 1, 3, and 6) are observed in the respective PE spectrum.[5] In the experiment, the intensity of the band near the threshold decreases systematically with increasing Ag concentration. Simultaneously, new states with increasing intensity appear between 0.5–2.0 eV. Importantly,

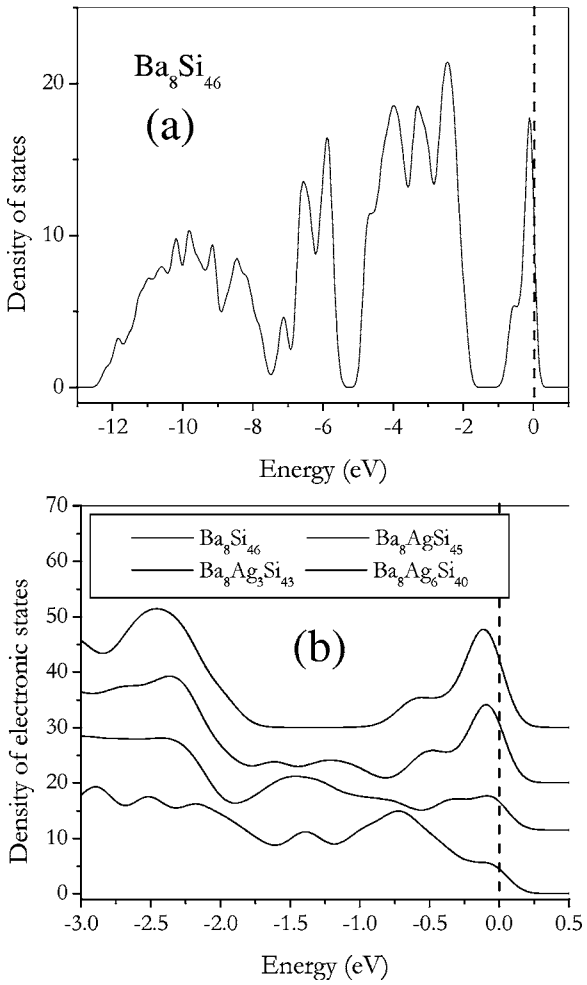

FIG. 1. Calculate electronic density of states for [(a), top] Ba_8Si_{46} in the energy range from −12 eV to 0 eV; [(b), bottom] for Ba_8Si_{46}, $Ba_8Ag_6Si_{40}$, and $Ba_8Au_6Si_{40}$ near the Fermi level. The dash lines indicate the position of the Fermi level.

the superconducting transition temperatures of $Ba_8Ag_nSi_{46-n}$ are found to correlate almost linearly with the integrated intensity of the first band.[5] The pure Ba_8Si_{46} is an 8 K superconductor but $Ba_8Au_6Si_{40}$ is a nonsuperconducting metal. This observation apparently supports the Bardeen-Cooper-Schrieffer (BCS) theory that the DOS at the Fermi level is the dominant factor responsible for the high superconducting transition temperature of Ba_8Si_{46}.

Changes in the profile of the electron density of states of $Ba_8Ag_nSi_{46-n}$ can be easily explained from the analysis of the band structures. The electron band dispersions for Ba_8Si_{46}, $Ba_8Ag_nSi_{46-n}$, and $Ba_8Au_6Si_{40}$ are shown in Figs. 2 and 3. For Ba_8Si_{46}, even though there is strong hybridization between the Ba and Si states, there is a "pseudo"-gap between −0.5 and −2.0 eV. This is reminiscent of the band gap in the pure[22,25] Si_{46} (Fig. 3). Replacement of the framework Si resulted in the filling of the "gap" with Ag states. The Ag *d* states also contribute to the narrow band between −5 and −6 eV. The gradual filling of the gap between −0.5 to −2.0 eV corresponds to the observed increase intensity of the PE bands in this energy region.[5] In contrast, the density of electronic bands near and below the Fermi level decreases significantly. In Si_{46} and Ba_8Si_{46} these bands are primarily Si-Si $3p$ "antibonding" orbitals. Removal of Si from the framework decreases the number of these orbitals resulting in a lower density of states at the Fermi level. The bonding in the $Ba_8Ag_nSi_{46-n}$ can be viewed in a different perspective. In a formal sense, each Si contributes four valence electrons for the tetrahedral bonding. Since Ag has an electronic configuration of $4d^{10}5s^1$, the replacement of a Si by Ag leads to an electron deficient compound where the full coordination cannot be satisfied. Therefore, the chemical bonding in $Ba_8Ag_nSi_{46-n}$ is fundamentally different from that of Ba_8Si_{46}. This has a strong effect on the vibrational properties as will be discussed below.

Finally, we compare the electronic structure of Ba_8Si_{46}, $Ba_8Ag_6Si_{40}$, and $Ba_8Au_6Si_{40}$. The calculated band structures for these compounds are shown in Fig. 2. As anticipated, the band structure for $Ba_8Ag_6Si_{40}$ and $Ba_8Au_6Si_{40}$ are very similar. $Ba_8Au_6Si_{40}$, as in $Ba_8Ag_6Si_{40}$, the Au *s* and *d* states are located in the gap region of Si_{46}. In both cases, the density of electronic states near the Fermi level is very low even though the bands at the Fermi level are quite flat. In fact, the band structure profiles resemble a weak metal.

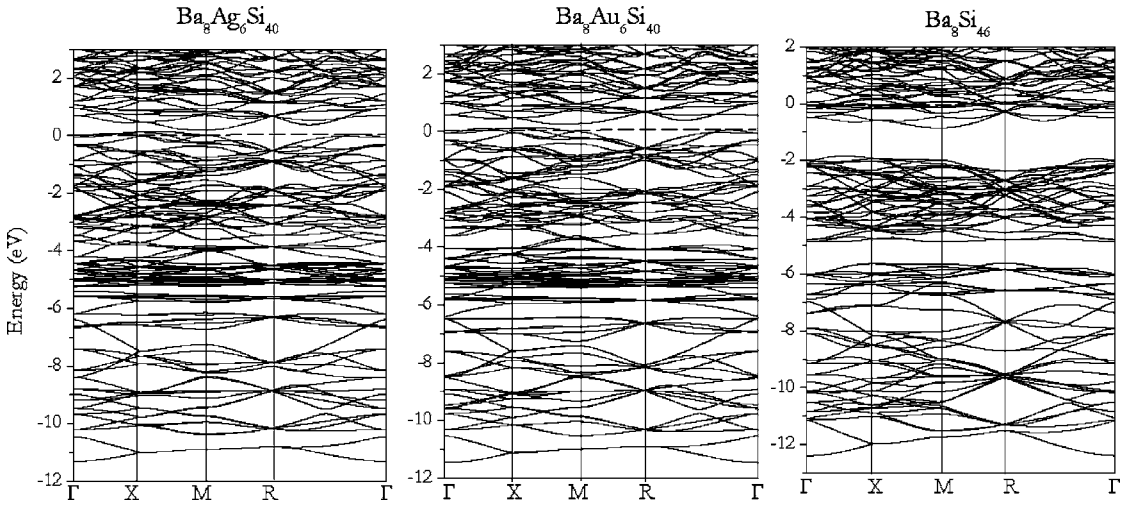

FIG. 2. Electronic band structure for (a) Ba_8Si_{46}, (b) $Ba_8Ag_6Si_{40}$, and (c) $Ba_8Au_6Si_{40}$.

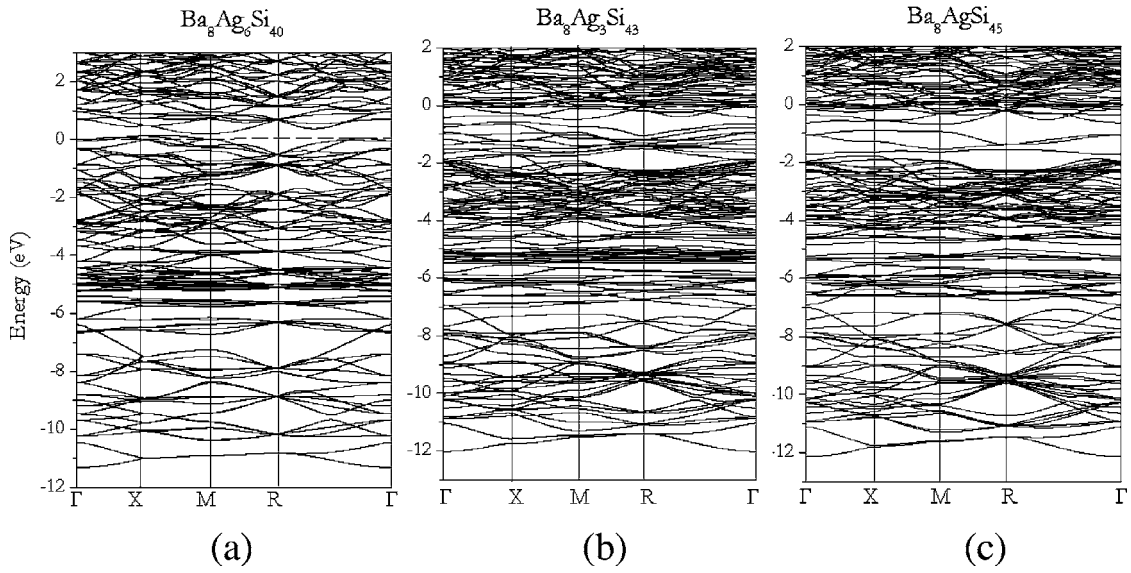

FIG. 3. Electronic band structure for (a) Ba_8AgSi_{45}, (b) $Ba_8Ag_3Si_{43}$, and (c) $Ba_8Ag_6Si_{40}$.

Therefore, the electrical properties of $Ba_8Ag_6Si_{40}$ and $Ba_8Au_6Si_{40}$ should be similar.

B. Vibrational properties

Before embarking on the discussion of the vibrational properties and the comparison of theoretical results with experimental Raman spectra, it is instructive to analyze the Si lattice modes in Ba_8Si_{46} in detail. The crystal symmetry of a type I Si clathrate is $Pm3n$ and there are three crystallographically distinct types of Si forming the framework. In the Wyckoff notation, these Si occupy the $6c$, $16i$, and $24k$ sites.[26] The vibrational density of states of the framework can be decomposed into the partial density of states (PDOS) for each type of Si atom. The results are shown in Fig. 4. Several pieces of important information can be obtained by studying the PDOS. First, Si atoms on the $6c$ sites do not contribute to the highest energy optical vibrational mode at $\sim$420 cm^{-1} at all. Furthermore, their contribution to the band at 350 cm^{-1} is also very minor. On the other hand, Si in the $16i$ sites are almost the sole contributor to the optical vibration at $\sim$420 cm^{-1}. Finally, the Si vibrational density of states shows a typical Debye-like behavior in the frequency region 0–50 cm^{-1} below the onset of the Ba vibrational bands.

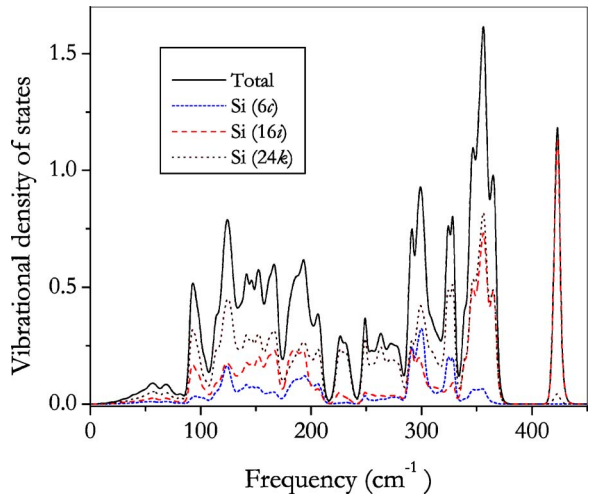

FIG. 4. (Color online) Calculated projected vibrational density of states for Si located in Wyckoff position $6c$, $16i$, and $24k$ of Ba_8Si_{46}. The density of states is normalized to $3n$, where N is the number of atoms.

Next we examine the Ba vibrations in Ba_8Si_{46}. In a type I clathrate, there are two types of cavities with different free volumes. There are two pentagonal dodecahedra (5^{12}) and six larger tetrakaidecahedra ($6^2 5^{12}$).[27] The PDOS for Ba in the two types of cages are shown in Figs. 6(a) and 7(a). Having a larger free volume, the vibrational frequencies of the Ba in the large cage ($\sim$55 cm^{-1}) are lower than those encapsulated in the small cages (70–115 cm^{-1}). Although the site symmetry of the small cages ($m\bar{3}$) is higher than that of the large cages ($\bar{4}m2$),[26] we observed a large splitting of the vibrations spreading from 70 to 115 cm^{-1}. These are strong indications that interactions with the host Si framework are much stronger for the Ba in the small cages than in the large cages. On closer examination [Fig. 7(a)], we found that the Ba in the small cages also mixed with the lattice modes at $\sim$250–350 cm^{-1} and also to the highest frequency band at 420 cm^{-1}. The strong mixing of the "guest" metal and "host" Si framework vibrations is very different from that observed in Na_8Si_{46}.[19] In the latter case, the Na vibrations are much more localized and decoupled from the lattice modes except in regions where there is symmetry-forbidden avoided anticrossing. The difference in the vibrational behavior is obviously the consequence of strong hybridization of the Ba electronic states with the conduction bands of the Si_{46} framework.

The conclusion drawn from the analysis of the PDOS is in complete agreement with the phonon band structure. In Fig. 5(a), it is shown $\sim$55–60 cm^{-1} at the zone center (Γ), there

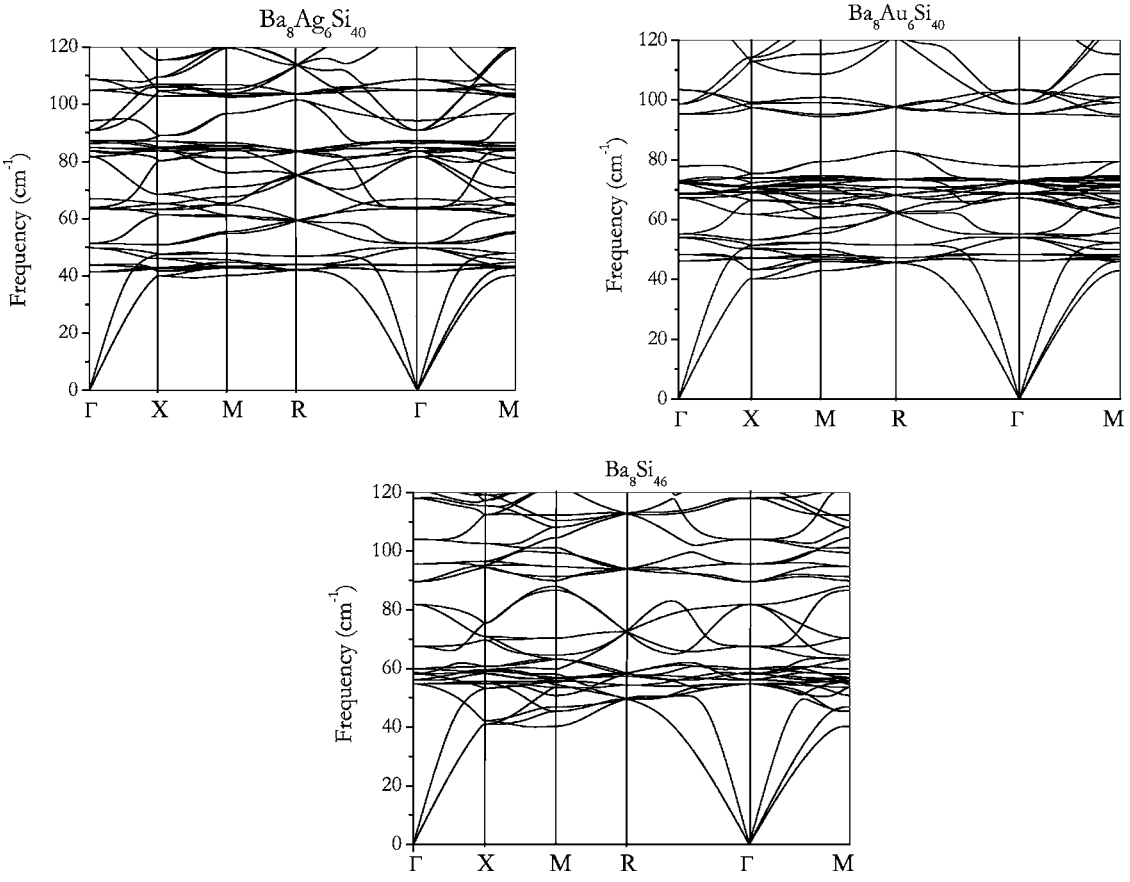

FIG. 5. Calculated phonon band structure for (a) Ba_8Si_{46}, (b) $Ba_8Ag_6Si_{40}$, and (c) $Ba_8Au_6Si_{40}$.

is a narrow band of predominantly Ba vibrations in the large cages. This band corresponds to the peak centered at 55 cm^{-1} in the PDOS. In comparison to Na_8Si_{46},[19] the Ba modes in the large cage show much stronger dispersion along the $\Gamma \rightarrow X \rightarrow M \rightarrow R$ direction. Therefore, even though apparently a single band was observed in the PDOS, it does not indicate that the Ba atoms in the large cages are localized oscillators. Vibrations in the small cages at higher frequencies show even larger dispersion.

The replacement of the Si in the 6*c* sites with Ag or Au has a dramatic effect on the vibrational spectra. The most interesting observation is that the Ba vibrations shift to lower frequencies and split into three distinct bands [Figs. 6(b) and 6(c)]. In $Ba_8Ag_6Si_{40}$, the two lowest energy bands at 43 and 63 cm^{-1} [Fig. 7(b)] are associated with Ba in the large cages. The PDOS profile and the intensity ratio of almost 2:1 remind us of the localized vibrational profile of rare gas trapped in the type I clathrate hydrate.[28,29] The dispersion of these phonon bands are relatively flat indicating that interactions with the lattice modes are small. The PDOS for Ba in the small cages shows four peaks at 71, 83, 105, and 134 cm^{-1} with the strongest peak at 105 cm^{-1}. Inspection of the phonon band structure shows there are a few flat bands at $\sim$105 cm^{-1}. The Ba vibrations in the small cage also mix more strongly with higher energy Si lattice vibrations than the vibrations in the large cage, particularly at 200, 309, and 402 cm^{-1}. Incidentally, the PDOS of the Ba vibrations in the small cages overlaps with the features observed in the Ag PDOS [Fig. 6(b)]. The highest density of states for the Ag vibrations is observed at 83 cm^{-1}. Since the Ag atoms are now components of the clathrate framework, their motions mixed strongly with Si lattice vibrational modes at 138, 200, 240, and 280 cm^{-1}. The substitution of Si in the 6*c* sites by Ag reduces the interactions of the framework atoms with Ba in the large cages but maintains similar interactions as in Ba_8Si_{46} for Ba in the small cages. Since the Si atoms at the 6*c* sites do not contribute to the high frequency optical mode, the effect of substitution is the shift of the peak at 430 cm^{-1} in Ba_8Si_{46} to 400 cm^{-1}. The red shift can be explained by a weakening of the Si–Si bonds since, as described above, the clathrate framework becomes electron deficient when the Si are substituted by Ag.

The vibrational DOS for $Ba_8Au_6Si_{40}$ shares many similar features with $Ba_8Ag_6Si_{40}$ [Figs. 6(c) and 7(c)]. In comparison to $Ba_8Ag_6Si_{40}$, the vibrations of Ba in the large cages shift to slightly higher energy (by a few wave numbers). The major difference is that the Au vibrational modes shift to a lower frequency. The maximum of the Au PDOS is located at $\sim$70 cm^{-1} [Fig. 7(c)]. The mixing of the vibrations of Au with Ba in the small cages is very clear. In contrast, the highest frequency peak shifted up by 11 cm^{-1} to 411 cm^{-1}.

The experimental Raman spectra for Ba_8Si_{46},[10] $Ba_8Ag_6Si_{40}$, and $Ba_8Au_6Si_{40}$ are shown in Fig. 8. Strictly speaking, a direct comparison of a Raman spectrum with calculated vibrational density of states is not appropriate. The observable Raman peaks of a crystalline material are

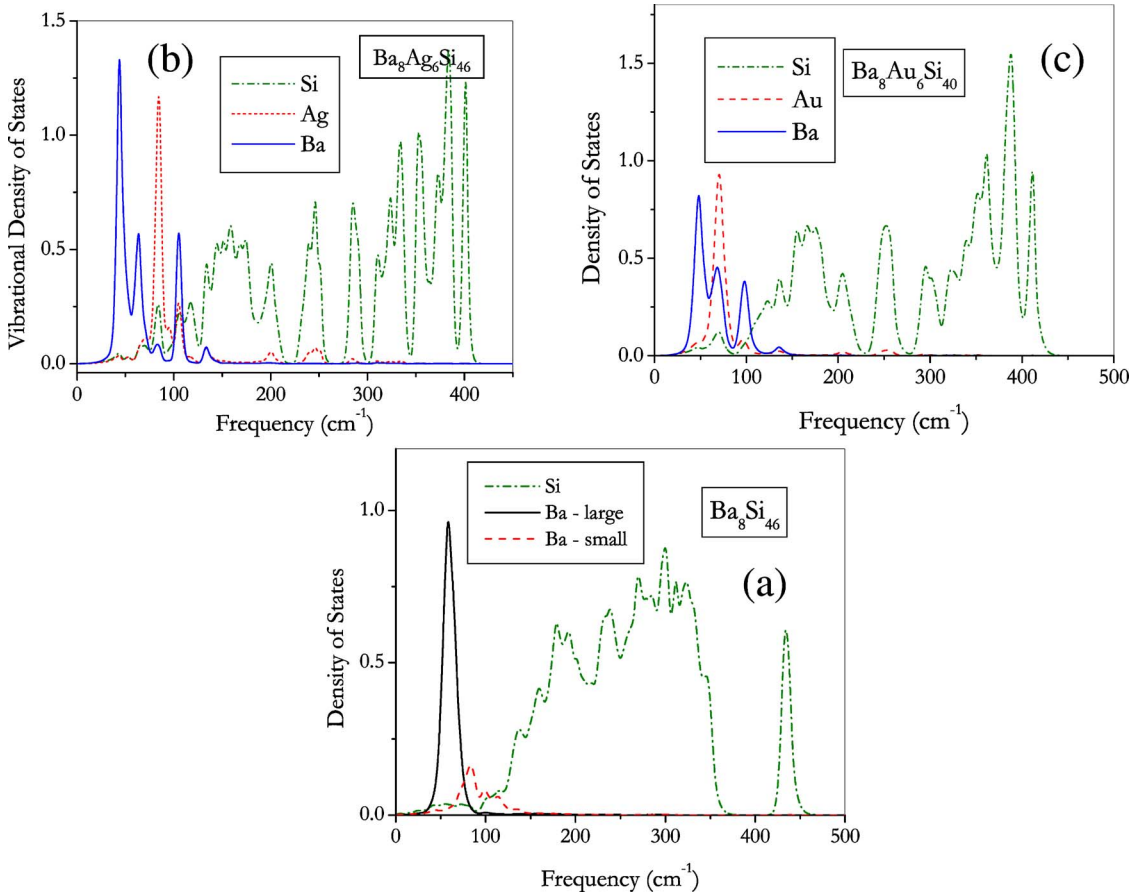

FIG. 6. (Color online) Calculated projected vibrational density of states for (a) Ba_8Si_{46}, (b) $Ba_8Ag_6Si_{40}$, and (c) $Ba_8Au_6Si_{40}$.

governed by symmetry selection rules. In addition, only zone center phonons can be observed. In contrast, vibration DOS includes all phonon modes and the intensity is dependent on details of the phonon band structure and is more sensitive to zone boundary phonons where the dispersions are usually small. In Ba_8Si_{46} and $Ba_8Au_6Si_{40}$, the highest energy band is observed at 438 cm^{-1} and 407 cm^{-1}, respectively.[10] This is in excellent agreement with the theoretical predicted vibrations 434 cm^{-1} and 411 cm^{-1}, respectively. Other high energy bands observed in Ba_8Si_{46} at 153, 255, 311, and 346 cm^{-1} correlate reasonably well with distinctive features in the calculated vibrational DOS at 159, 269, 301, and 344 cm^{-1}. At the low frequency region below 100 cm^{-1}, three strong peaks at 49, 60, and 89 cm^{-1} and perhaps a weaker structure at 73 cm^{-1} were observed. From a factor group analysis[21,30] it was shown that there are no Raman active Ba atom vibrations in the small cages of type I clathrate. Therefore, the observed lower energy peaks are likely due to Ba vibrations in the large cages. In this energy region, calculations predicted the following Raman active modes: T_{2g} at 54.6 cm^{-1}. E_g at 55.4 cm^{-1}, T_{2g} at 78, and E_g at 88 cm^{-1}.

When the Si 6*c* sites are replaced by Au or Ag atoms, the position of the highest energy peak shifts to lower energy. In $Ba_8Au_6Si_{40}$ the calculated frequency of 411 cm^{-1} is again in excellent agreement with the experimental value of 407 cm^{-1}. A major difference between the Raman spectra of Ba_8Si_{46} and $Ba_8Ag_6Si_{40}$ or $Ba_8Au_6Si_{40}$ is the "disappearance" of the strong peak at 153 cm^{-1}. The obvious explanation is that this peak must be due to the vibrations of the Si at the 6*c* sites. The peaks observed at 252 and 299 cm^{-1} in $Ba_8Ag_6Si_{40}$ are probably associated with the calculated features in the DOS at 246 and 285 cm^{-1}. In the low-frequency region, the predominantly Ba vibrations become sharper in the Raman spectra. In $Ba_8Ag_6Si_{40}$, a series of peaks and shoulders are identified at 51, 58, 74, 84, 95, and 105 cm^{-1}. In comparison with the calculated DOS, the two lowest strong peaks (51 and 74 cm^{-1}) may be the vibrations of Ba in the large cages predicted at 43 and 64 cm^{-1}. The band observed at 84 cm^{-1} is probably correspond to the Ag vibrations calculated at 82 cm^{-1}. The bands at 95 and 105 cm^{-1} may be assigned to Ag and Si mixed vibrations. The low-frequency region of $Ba_8Au_6Si_{40}$ can be assigned in a similar manner. The lowest energy band at 51 cm^{-1} and the clear shoulder at 70 cm^{-1} are assigned to the vibrations of Ba in the large cages with calculated positions of 48 $cm^{-1}(T_{2g})$ and 68 $cm^{-1}(E_g)$. The strong Raman peak at 75 cm^{-1} is assigned to the Au band calculated at 70 $cm^{-1}(E_g)$ and 71 $cm^{-1}(T_{2g})$. The observed band at 96 cm^{-1} is very close to the calculated T_{2g} Au vibrations at 96 cm^{-1} in the DOS. The consistent agreement between theory and experiment lend support to the assignments proposed here.

Figure 9 shows changes in the Raman spectra in the series $Ba_8Au_nSi_{46-n}$ (n=0,1,3–6). The gradual shift of the highest energy band from Ba_8Si_{46} to $Ba_8Au_6Si_{40}$ with increasing Au substitution is evident. There are also several interesting spectral features. For example, the very strong Raman peak

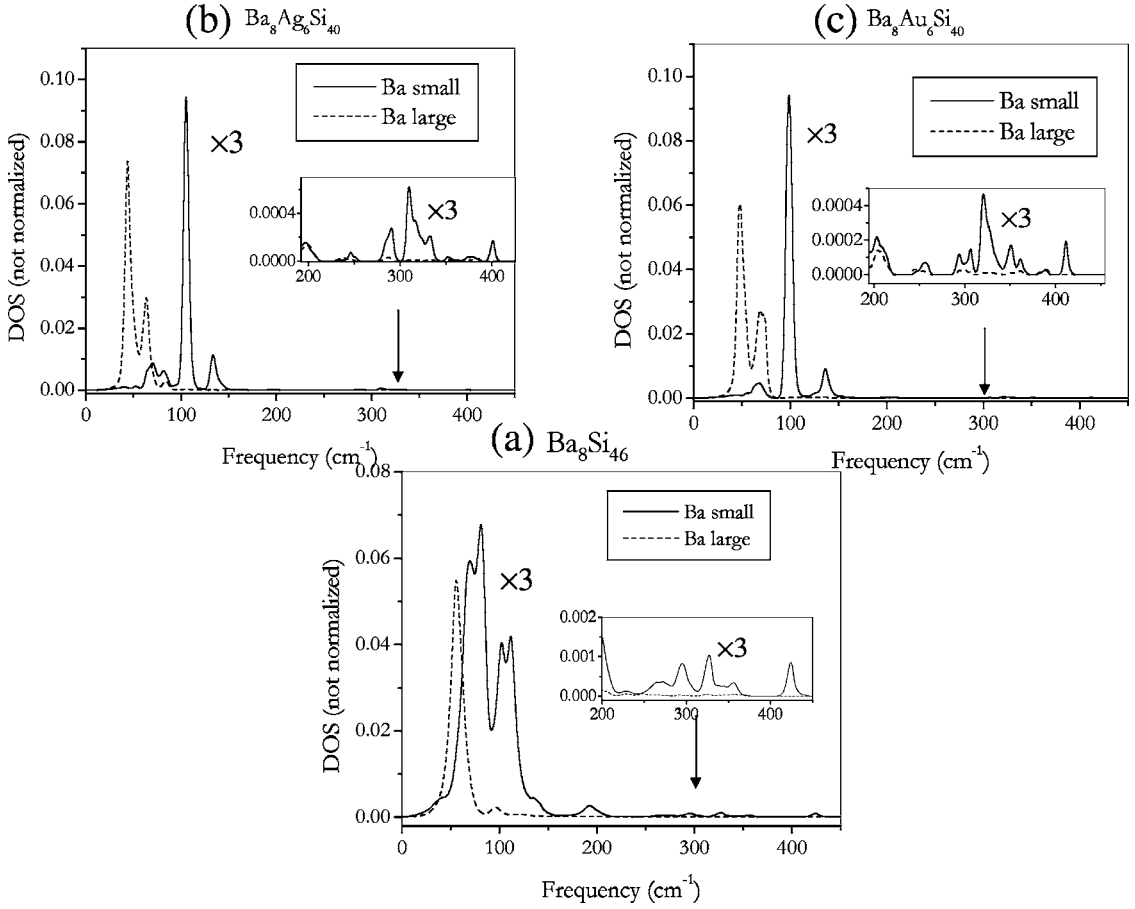

FIG. 7. Detail analysis of the vibrational density of states of the Ba atoms encapsulated in the small and large cages of (a) Ba_8Si_{46}, (b) $Ba_8Ag_6Si_{40}$, and (c) $Ba_8Au_6Si_{40}$.

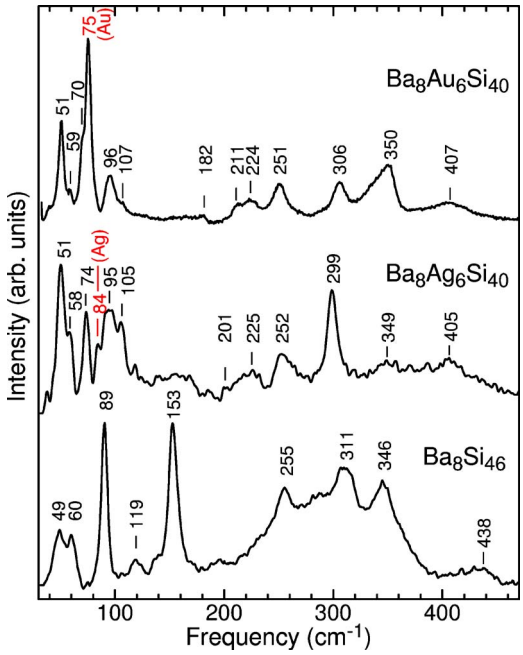

FIG. 8. (Color online) Experimental Raman spectra for (a) Ba_8Si_{46}, (b) $Ba_8Ag_6Si_{40}$, and (c) $Ba_8Au_6Si_{40}$.

at 153 cm^{-1} in Ba_8Si_{46} lost its intensity immediately upon substitution. In contrast, the intensity of the Raman bands at 255, 311, and 346 in Ba_8Si_{46} is reduced in $Ba_8Au_nSi_{46-n}$ ($n=1$ and 3) but becomes much sharper at higher levels of Au substitution. The loss in intensity may be due to positional disordering at a low level of Au substitution, which recovers at higher Au substitution. There are also significant changes in the Raman profile in the frequency region below 100 cm^{-1}. The Au vibrational peak (solid circle) is enhanced with the Au substitution. The Ba related vibrations (49, 60, and 89 cm^{-1} in Ba_8Si_{46}) are also strongly affected, suggesting the evolution of the interaction of Ba with the framework.

C. Superconductivity in Ba_8Si_{46}

Recently, an investigation on the mechanism for the superconductivity in the polyhedral covalent Ba-doped Si clathrate, Ba_8Si_{46}, has been reported.[6] Measurements of the $^{28}Si/^{30}Si$ isotopic effect on magnetic susceptibility and the low temperature specific heat show convincingly that Ba_8Si_{46} is a normal BCS *s*-wave superconductor.[6] However, the assignments of the Raman spectra need to be scrutinized as it has led to incorrect conclusions. As indicated above, previous studies and the results presented here show that there are significant hybridizations in the electronic bands leading to

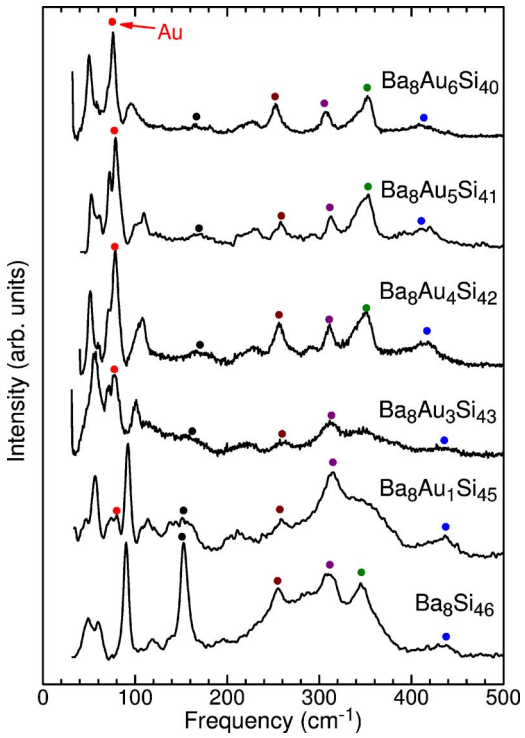

FIG. 9. (Color online) Experimental Raman spectra for $Ba_8Au_nSi_{46-n}$ (n=0, 1, and 3–6).

mixing of the vibrations of the metal vibrations with Si_{46} lattice phonons when doped with heavy metal. Therefore, no highly localized Ba vibrations exist at the frequency suggested in the previous report.[6] First-principles phonon calculations [Fig. 6(a)] indicate that Ba motions dominate and only contribute to the low-frequency modes at 60 cm^{-1} and below 120 cm^{-1} (large and small cages, respectively). All vibrations above 150 cm^{-1} are attributed to Si vibrations. Moreover, phonon dispersions clearly show that these modes are mixed Ba and lattice acoustic phonons and cannot be described as localized vibrations.[2] The predicted trend in the isotopic frequency shift is also in excellent agreement with the experiment.[1] The calculated shift is -15 cm^{-1} for the optical mode at 423 cm^{-1} and -10 cm^{-1} for the 191 cm^{-1} band. In contrast, it is only -4 cm^{-1} for the 251 cm^{-1} band. Since there are different mixings of Ba components, even for Si-dominating vibrations, the isotopic effect need not be the same and should not always proportional to $(^{28}m_{Si}/^{30}m_{Si})^{1/2}$ $\sim$0.97. Thus, the assignment of the 252 cm^{-1} Raman peak to a dominant Ba mode is not valid. The argument that the high energy optic band at 437 cm^{-1} is strongly affected by Cooper pairing is also incorrect. Substituting some of the framework Si with Au increases the reduced mass and a weakened Au-Si interaction leading to a decrease in the lattice frequencies. Phonon calculations indeed show that the 423 cm^{-1} optical mode in Ba_8Si_{46} is lowered to 411 cm^{-1} in $Ba_8Au_6Si_{40}$. The depression of the superconducting temperature in $Ba_8Au_6Si_{40}$ cannot be related to this mode.

To further explore the role of the guest atom to the superconductivity property, contributions from each type of atom in Ba_8Si_{46} to the electron-phonon coupling parameter $\lambda(\omega)$ were calculated and the results are shown in Fig. 10. These

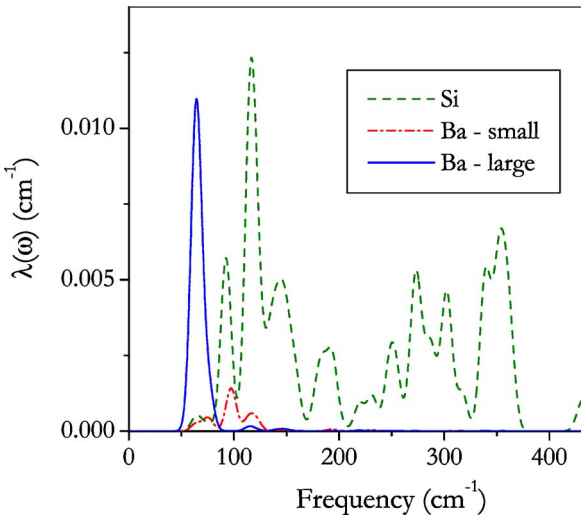

FIG. 10. (Color online) Electron-phonon coupling parameter $\lambda(\omega)$ of Ba_8Si_{46} decomposed into contributions from Si atoms and Ba in small and large cages.

calculations were based on the density functional perturbation theory[31] employing the Perdew-Burke-Ernzerhof generalized-gradient approximation (PBE-GGA) functional with a plane wave cutoff energy of 30 Ry and a $2\times2\times2$ Monkhorst-Pack k-point set for geometry optimization and phonon calculations. A slightly larger $4\times4\times4$ k-point set was used for the calculation of electron-phonon interactions. In view of the computational cost, only zone center phonons are considered. Therefore, the calculations may not be accurate enough to provide a quantitative value for λ, however this is sufficient to illustrate the relative contribution from each phonon modes at the zone center. The calculated overall $\lambda(\omega)$[30] is in close agreement with the previous report.[7] As shown in Fig. 10, the lattice Si vibrations contribute over the entire frequency range. However, contributions from phonon modes at 250 cm^{-1} and 435 cm^{-1} are quite minor. This observation reinforces the comments presented above (*vida infra*). Largest contributions to the spectral function are from Si lattice phonon modes overlapping with the Ba vibrations in the small cages. Surprisingly, the corresponding Ba atoms in the small cavities only made minor contributions. In contrast, contributions from the Ba vibrations in a large cage, though not dominant, are still very significant. Since the electron-phonon coupling parameter is proportional to the first inverse moment of the spectral function,[32] the larger contribution from the Ba in the large cages may be attributed to their lower energy vibrations. Using the theoretical frequency spectrum and assuming a superconducting isotopic coefficient $\alpha\sim0.08$ to 0.12,[1,6] we found $\lambda=1.08$–1.13 and $\mu^*=0.27$–0.29. These values are consistent with previous estimates.[1,6,7] The larger than usual μ^* is significant as it may indicate more complicated mechanisms to superconductivity. The analysis presented here complements the results reported earlier.[7] In passing, it should be noted that the present calculations as well as Raman spectroscopy only explore phonon modes at the zone center. Phonons in entire Brillion zone may also contribute to the superconductivity. It is obvious that the understanding of the electron-phonon coupling in

superconducting metal-doped Si clathrates is still incomplete and further investigations are needed.

IV. CONCLUSIONS

The electronic structure and vibrational dynamics of Ba_8Si_{46} and $Ba_8(Ag,Au)_nSi_{46-n}$ ($n=1$–6) has been characterized through first-principles calculations and the analysis of the Raman spectra. The experimental observation of the reduction in the electron density at the Fermi level is fully substantiated by the theoretical calculations. It is shown that when the framework Si atoms are replaced by Ag or Au atoms, the clathate frameworks become electron deficient. Consequently, the electronic structures differ substantially from pure Ba_8Si_{46}. The Ba atoms, especially those encapsulated in the small cavities of the clathrate structure, interact strongly with the Si framework. As a result, in contrast to Na_8Si_{48} the Ba vibrations cannot be treated as localized "rattling" motions. This conclusion is similar to a previous theoretical investigation on the motions of $(Ge,Ga)_{46}$ clathrates containing group I and II elements in their cavities.[33] The interactions between Ba in the large cages and the framework seem to diminish with the substitution with Ag and Au. The vibrational bands observed in the Raman spectra can be assigned reasonably well to major features in the calculated vibrational density of states.

ACKNOWLEDGMENT

The authors wish to thank the Advanced Center for Computing and Communication, RIKEN for the generous allotment of computational resources on the RIKEN Super Combined Clusters (RSCC) system where all the calculations reported in this work were performed.

[1] H. Kawaji, H. O. Horie, S. Yamanaka, and M. Ishikawa, Phys. Rev. Lett. **74**, 1427 (1995).
[2] S. Yamanaka, E. Enishi, H. Fukuoka, and M. Yasukawa, Inorg. Chem. **39**, 56 (2000).
[3] P. Toulemonde, Ch. Adessi, X. Blasé, A. San Miguel, and J. L. Tholence, Phys. Rev. B **71**, 094504 (2005).
[4] Y. Nozue, G. Hosaka, E. Enishi, and S. Yamanaka, Mol. Cryst. Liq. Cryst. Sci. Technol., Sect. A **341**, 509 (2000).
[5] N. Kamakura, T. Nakano, Y. Ikemoto, M. Usuda, H. Fukuoka, S. Yamanaka, S. Shin, and K. Kobayashi, Phys. Rev. B **72**, 014511 (2005)
[6] K. Tanigaki, T. Shimizu, K. M. Itoh, J. Teraoka, Y. Moritomo, and S. Yamanaka, Nat. Mater. **2**, 653 (2003).
[7] D. Connetable, V. Timoshevskii, B. Masenelli, J. Beille, J. Marcus, B. Barbara, A. M. Saitta, G-M. Rignanese, P. Mélinon, S. Yamanaka, and X. Blasé, Phys. Rev. Lett. **91**, 247001 (2003).
[8] W. L. McMillan, Phys. Rev. **167**, 331 (1968).
[9] E. Reny, A. San-Miguel, Y. Guyot, B. Masenelli, P. Mélinon, L. Saviot, S. Yamanaka, B. Champagnon, C. Cros, M. Pouchard, M. Borowski, and A. J. Dianoux, Phys. Rev. B **66**, 014532 (2002).
[10] T. Kume, H. Fukuoka, T. Koda, S. Sasaki, H. Shimizu, and S. Yamanaka, Phys. Rev. Lett. **90**, 155503 (2003).
[11] H. Fukuoka, J. Kiyoto, and S. Yamanaka, Inorg. Chem. **42**, 2933 (2003).
[12] R. F. W. Herrmann, K. Tanigaki, S. Kuroshima, and H. Suematsu, Chem. Phys. Lett. **283**, 29 (1998).
[13] R. F. W. Herrmann, K. Tanigaki, T. Kawaguchi, S. Kuroshima, and O. Zhou, Phys. Rev. B **60**, 13245 (1999).
[14] G. Kresse and J. Furthmüller, Comput. Mater. Sci. **6**, 15 (1996); G. Kresse and J. Furthmüller, Phys. Rev. B **54**, 11169 (1996).
[15] G. Kresse and D. Joubert, Phys. Rev. B **59**, 1758 (1999).
[16] K. Parlinski, Z. Q. Li, and Y. Kawazoe, Phys. Rev. Lett. **78**, 4063 (1997).
[17] Z. Li and J. S. Tse, Phys. Rev. B **61**, 14531 (2000).
[18] G. Kresse, J. Furthmüller, and J. Hafner, Europhys. Lett. **32**, 729 (1995).
[19] J. S. Tse, Z. Q. Li, and K. Uehara, Europhys. Lett. **56**, 261 (2001).
[20] J. Dong, O. F. Sankey, A. A. Demkov, G. K. Ramachandran, J. Gryko, P. F. McMillan, and W. Windl, Mater. Res. Soc. Symp. Proc. **545**, 443 (1999).
[21] L. Qiu, M. A. White, Z. Li, J. S. Tse, C. I. Ratcliffe, C. A. Tulk, J. Dong, and O. F. Sankey, Phys. Rev. B **64**, 024303 (2001)
[22] S. Baroni, A. Dal Corso, S. de Gironcoli and P. Giannozzi, http://www.pwscf.org
[23] P. Ordejón, E. Artacho, and J. M. Soler, Phys. Rev. B **53**, R10441 (1996); J. M. Soler, E. Artacho, J. D. Gale, A. García, J. Junquera, P. Ordejón, and D. Sánchez-Portal, J. Phys.: Condens. Matter **14**, 2745 (2002).
[24] K. Moriguchi, M. Yonemura, A. Shintani, and S. Yamanaka, Phys. Rev. B **61**, 9859 (2000).
[25] J. S. Tse, K. Uehara, R. Rousseau, A. Ker, C. I. Ratcliffe, M. A. White, and G. MacKay, Phys. Rev. Lett. **85**, 114 (2000).
[26] See, e.g., http://www.cryst.ehu.es/
[27] J. R. Ripmeester, C. I. Ratcliffe, D. D. Klug, and J. S. Tse, Ann. N.Y. Acad. Sci. **715**, 161 (1994).
[28] J. S. Tse and M. L. Klein, J. Chem. Phys. **78**, 2096 (1983).
[29] J. S. Tse, V. P. Shpakov, V. R. Belosludov, F. Trouw, Y. P. Handa, and W. Press, Europhys. Lett. **54**, 354 (2001).
[30] J. S. Tse, C. I. Ratcliffe, B. M. Powell, V. F. Sears, and Y. P. Handa, J. Phys. Chem. A **101**, 4491 (1997).
[31] S. Baroni, S. de Gironcoli, A. Dal Corso, and P. Giannozzi, Rev. Mod. Phys. **73**, 515 (2001).
[32] S. Y. Savrasov and D. Y. Savrasov, Phys. Rev. B **54**, 16487 (1996).
[33] J. J. Dong, O. F. Sankey, G. K. Ramachandran, and P. F. McMillan, J. Appl. Phys. **87**, 7726 (2000).